Supplemental Information:

Computational Analysis of Deposition and Translocation of Inhaled Nicotine and Acrolein in the Human Body with E-cigarette Puffing Topographies

Ahmadreza Haghnegahdar[1], Yu Feng[1,*], Xiaole Chen[2], Jiang Lin[3]

[1] School of Chemical Engineering, Oklahoma State University, Stillwater, OK, 74078, USA
[2]School of Energy and Environment, Southeast University, Nanjing, 210096, China
[3] Zhejiang University of Science and Technology, Hangzhou, 310023, China

S.1. Governing Equations

S.1.1 Computational Fluid-Particle Dynamics (CFPD)

S.1.1.1 Governing Equations for Air-Vapor Mixture

Assuming EC vapor species are diluted suspensions in the air, the air-vapor mixture can be modeled as a single continuous phase. Neglecting the evaporation effects of EC droplets, the governing equations of the air-aerosol mixture can be given as:

Continuity Equation

$$\frac{\partial u_i}{\partial x_i} = 0 \tag{S1}$$

in which u_i represents the i-th component of the continuous phase velocity.

Navier-Stokes (N-S) Equation

$$\rho\left(\frac{\partial u_i}{\partial t} + u_j\frac{\partial u_i}{\partial x_j}\right) = -\frac{\partial p}{\partial x_i} + \mu\frac{\partial^2 u_i}{\partial x_j^2} + \rho g_i \tag{S2}$$

where ρ and μ are the air-vapor mixture density and viscosity, respectively.

At typical puffing flow rates, airflow through the oral airway region and first few generations is incipient turbulent, becoming laminar again at from G4. Therefore, the shear stress transport (SST) transition model (Menter, Langtry, & Völker, 2006; Menter et al., 2006) is adapted in this study, based on its overall good performance on the prediction of "laminar-to-turbulent" transition onset, computational efficiency and reasonable accuracy when compared to large eddy simulation (LES). Based on the k-ω model, the SST transition model can be described as follows:

$$\frac{\partial}{\partial t}(\rho k) + \frac{\partial}{\partial x_i}(\rho u_i k) = \frac{\partial}{\partial x_i}\left((\mu + \mu_t/\sigma_k)\frac{\partial k}{\partial x_i}\right) + \tilde{G}_k - Y_k \tag{S3}$$

$$\frac{\partial}{\partial t}(\rho\omega) + \frac{\partial}{\partial x_i}(\rho u_i \omega) = \frac{\partial}{\partial x_i}\left((\mu + \mu_t/\sigma_\omega)\frac{\partial \omega}{\partial x_i}\right) + Cd_\omega + G_\omega - Y_\omega \tag{S4}$$

*Corresponding author. Tel: +1-405-744-7441; Fax: +1-405-744-6338
Email address: yu.feng@okstate.edu (Y. Feng)

$$\frac{\partial}{\partial t}(\rho\gamma) + \frac{\partial}{\partial x_i}(\rho u_i \gamma) = \frac{\partial}{\partial x_i}\left((\mu + \mu_t/\sigma_f)\,\frac{\partial \gamma}{\partial x_i}\right) + G_\gamma - Y_\gamma \tag{S5}$$

$$\frac{\partial}{\partial t}(\rho \tilde{R}e_{\theta t}) + \frac{\partial}{\partial x_i}(\rho u_i \tilde{R}e_{\theta t}) = \frac{\partial}{\partial x_i}\left(\sigma_{\theta t}(\mu + \mu_t)\,\frac{\partial \tilde{R}e_{\theta t}}{\partial x_i}\right) + G_{\theta t} \tag{S4}$$

In Eqs. (S3)-(S6), G and Y represent generation and dissipation of the turbulence kinetic energy (k) and the specific rate of the dissipation (ω). C_d parameter shows the cross-diffusion term, and σ is the Prandtl number. Also, the μ_t is the turbulent viscosity. The transported Reynolds number ($\tilde{R}e_{\theta t}$) in Eq. (S6) is used to find the intermittency generation term in Eq. (S5).

S.1.1.2 Governing Equations for Multi-component EC Particles

In this study, the one-way coupled Euler-Lagrange method is employed to predict the transport of inhaled EC particles (Feng et al., 2016). Due to the relatively small size of the particles, rotational motions are neglected. Particle diameter changes due to condensation, evaporation, or coagulation are not considered. The translation equation of particles can be given as:

$$m_p \frac{du_{p,i}}{dt} = F^D_{p,i} + F^L_{p,i} + F^{BM}_{p,i} + F^G_{p,i} \tag{S7}$$

where $F^D_{p,i}$, $F^L_{p,i}$, $F^{BM}_{p,i}$, and $F^G_{p,i}$ are drag force, Saffman lift force, Brownian motion induced force, and gravity. Basset force is neglected due to negligible size of particles compared to the fluid flow domain. Specifically, the drag force can be give as:

$$\vec{F}^D_p = \frac{1}{8}\pi\rho(\vec{u} - \vec{u}_p)\left|\vec{u} - \vec{u}_p\right| d_p^2 C_D / C_C \tag{S8}$$

$$C_D = \frac{24}{Re_p}(1 + 0.15\,Re_p^{0.687}) \tag{S9}$$

in which d_p is the particle diameter. In Eq. (S9), C_D is the drag force coefficient. $C_C$is the Cunningham correction factor (Allen & Raabe, 1985) which is defined as:

$$C_C = 1 + \frac{2\lambda}{d_p}(1.257 + 0.4e^{-1.1\frac{d_p}{2\lambda}}) \tag{S10}$$

where λ=65 nm represents the air mean free path. As long as the particle`s diameter compared to the characteristic length of the continuous phase domain is significantly small, the particle Reynolds number Re_p based on the difference between the particle and the airflow velocity is small enough, and the Saffman lift force can be calculated by Li and Ahmadi (1992):

$$\vec{F}^L_p = \frac{2K\,de_{ij}\,\nu^{1/2}}{(\rho_p/\rho)d_p(de_{lk}de_{kl})^{1/4}}(\vec{u} - \vec{u}_p) \tag{S11}$$

In Eq. (S11), de_{ij} is the deformation rate tensor (Drew, 1976).

Employing the Gaussian white noise process model provided by Li and Ahmadi (1992), The Brownian motion induced force can be expressed as:

$$\vec{F}_p^{BM} = \vec{G}\sqrt{\frac{\pi S_0}{\Delta t}} \tag{S12}$$

$$S_0 = \frac{216\nu k_B T}{\pi^2 \rho d_p^5 (\frac{\rho_p}{\rho})^2 C_C} \tag{S13}$$

In Eq. (S12), $\vec{G}$ is a three dimensional vector consisting of three independent zero-mean, unit-variance Gaussian random numbers ranging from 0 to 1. In Eq. (S13), S_0 is the spectral intensity, k_B is Boltzmann constant (1.38×10^{-23} J/K) and T is temperature which is equal to constant value of 310.15 K in this study.

For the simulation process, as suggested by Gupta and Peters (1985) the particle time step Δt_p should be larger than the time step needed for the particle and fluid molecules collision and smaller than relaxation time for interaction and external forces. Thus, Δt_p can be estimated using the following equation:

$$\Delta t_p = \left(\frac{3\pi \mu d_p}{C_c m_p}\right)^{-1} \tag{S14}$$

The regional deposition of particles in human airways can be quantified using deposition fraction (DF) and deposition efficiency (DE), which are defined as:

$$DF = \frac{Number\ of\ regional\ deposited\ particles}{Number\ of\ particles\ entering\ the\ mouth} \tag{S15}$$

$$DE = \frac{Number\ of\ regional\ deposited\ particles}{Number\ of\ particles\ entering\ the\ region} \tag{S16}$$

The deposition on the lung airway walls was considered to happen when the distance between the particle centroid and the airway wall is less than $0.5d_p$.

S.1.1.3 Convection-Diffusion Equations for EC Vapor Species

The convection-diffusion equations are introduced for those EC chemical compounds in vapor forms to describe the transport dynamics by tracking the material mass fractions in human respiratory systems. The generalized equation can be given as:

$$\frac{\partial Y_s}{\partial t} + \frac{\partial (u_i Y_s)}{\partial x_i} = \frac{\partial}{\partial x_i}\left[D_{a,s}\frac{\partial Y_s}{\partial x_i}\right] \tag{S17}$$

where Y_s is the mass fraction of species s and $D_{a,s}$ is the binary diffusivity of species s in the air.

The mixed boundary condition is developed for a more realistic vapor absorption boundary condition at airway walls, i.e.,

$$\Psi_s^{-1}\frac{\partial Y_{s,c}}{\partial x_i} = (Y_{s,f} - Y_\infty) \quad \text{(S18)}$$

in which $Y_{s,c}$ and $Y_{s,f}$ are the mass fraction of the species s on the local mesh cell and face centroid respectively. Y_∞ is the mass fraction of the species in the systemic region which is assumed to be zero at initial condition as long as the reaction of the acrolein and formaldehyde are suggested to be high at the first contacting site. (ATSDR, 2007). The absorption coefficient Ψ_s is defined as:

$$\Psi_s = \frac{D_{w,s}}{D_{a,s}H_{c,s}H_m} \quad \text{(S19)}$$

where, and $H_{c,s}$ denote the diffusivity of the species in mucus layers and the Henry's constant respectively. For defining the Henry's constants the vapor phase has been consider as air and the mucus layer tissue site has been considered as water. In this way, the vapor liquid equilibrium for air-water system has been considered. Besides, H_m is the mucus layer thickness which is assumed to be constantly equal to average value of 10 μm covering all around the geometry domain wall boundaries (ICRP, 1994).

S.1.1.4. Boundary Conditions

Airflow Inlet Conditions with Realistic Puffing Topography

To implement the most representative and realistic puffing topographies for this study, puffing waveforms are proposed and employed based on experimental measurements in existing papers. Three standards available both for CCs and ECs for smoking machine setup are studied. Specifically, the pattern proposed by the world health organization (World Health Organization, 2012) is a square waveform with the flow rate of 35 mL per 2 seconds and the 60-second interval between two consecutive puffs, i.e., (35:2:60). The second CC puffing topography proposed by ISO and the Health Canada Intense (ISO/TR 19478-2, 2015) is 55 ml per 2 seconds with a 30-second interval between two consecutive puffs (55:2:30). Additionally, the third puffing standard for EC related research is 55 ml per 3 seconds with 30-second intervals between consecutive puffs (55:3:30) (CORESTA, 2014) Other efforts seeking for EC puffing topography standards are summarized as follows. Goniewicz et al. (2013) claimed an average puff volume of 70 ml for EC puffing, while (Robinson, Hensel, Morabito, & Roundtree, 2015) tested the puffing pattern of and reported that the mean puff duration is 3.5 seconds with a mean puff volume of 133 ml. Using the same experimental setup, Behar and Talbot (2015) provided the statistical results based on a 20-subject cohort. Their investigation shows that the average interval between two puffs is 179 seconds for puffs with an average duration of 2.65 seconds and volume of 51 ml. Furthermore, Dautzenberg and Bricard (2015) discovered that the puff duration increases slightly from 3.79 seconds to 4.11 seconds with the increase of the familiarity to EC consumption. Arguments exist on whether the observed longer puff duration is realistic or not. Longer puff duration and shorter puff interval will cause the formation of unpleasant tastes known as "dry puffs," which prevents the users to inhale EC aerosols too long to avoid the uncomfortableness.

(McAuley, Hopke, Zhao, & Babaian, 2012; Farsalinos, Voudris, & Poulas, 2015). On the other hand, CC users intend to puff longer and milder to inhale more nicotine in their lung (Feng et al., 2016).

Table S.1. Properties of the inhaled multicomponent EC aerosols (Margham et al., 2016).

Particle Diameter (nm)	500					
Temperature (K)	310					
Gas Mean free path (nm)	65					
Puffing topography (ml, s, s)	**55**:3:30					
	Acrolein	Formaldehyde	Nicotine	VG	PG	Water
EC Cartridge component (wt/wt)	0	0	1.86	48.14	25	25
Liquid mixture density (kg/m^3)	1238.9559					
Liquid mixture dynamic viscosity (kg/m s)	0.002682					
	Acrolein	Formaldehyde	Nicotine	VG	PG	Water
Generated vapor component per puff (wt/wt)	9.0373E-05	7.8897E-05	0.04590	2.29	1.02	N/A
Vapor mixture density (kg/m^3)	1.2530					
Vapor mixture dynamic viscosity (kg/m s)	1.8096E-05					
Puffing topography (ml, s, s)	**80**:3:30					
	Acrolein	Formaldehyde	Nicotine	VG	PG	Water
Generated vapor component per puff (wt/wt)	0.0001105	0.0001075	0.04590	2.29	1.02	N/A
Vapor mixture density (kg/m^3)	1.2530					
Vapor mixture dynamic viscosity (kg/m s)	1.8096E-05					

Based on the statistical data obtained from the open literature, three different inlet conditions are considered in this study. Specifically, two puffing volumes are considered, i.e., 55 and 80 ml, which are both with a 3-second puff duration. Moreover, the puffing interval (i.e., the holding and rest duration) also varies (see Table 1 for details). Poiseuille flow is assumed at the mouth inlet. Furthermore, constant body temperature T=310.15 K is considered in the human respiratory upper airway model. Simulation of the

transient, 3-second puffing duration followed by up to 7.0 s holding time is performed by discretizing the continuous particle injection. To find the best time interval between two consecutive particle injections, different time steps have been set up for the simulation, and the cumulative particle depositions in different regions were compared. Figures S.1 (a) and (b) depict the simulated cumulative deposition data at outlets and mouth to trachea walls respectively. The difference of the depositions for time step sizes of 0.02 s and 0.05 s are within 1.0%, hence for better computational performance, 0.05 s is selected as the final particle injection interval.

Particle and Vapor Inlet Conditions

Since the evaporation/condensation effects are neglected, the multi-component EC particles have the same composition as the e-liquid employed (Margham et al., 2016). Constant physical and chemical properties of EC chemical compounds are assumed. E-liquid composition provided by Margham et al. (2016) was used in this study. The EC aerosol mixture consists of 48.14% vegetable glycerin (VG), 25% of propylene glycol (PG), 25% water, 1.86% nicotine, and flavorings. The monodispersed particle diameter is assumed to be 410 nm, and the number concentration peak of 4.39e+9 particles per cm^3 is used. The choice of particle diameter and concentration are based on realistic EC aerosol measurements (Belka, Lizal, Jedelsky, Jicha, & Pospisil, 2017; Margham et al., 2016). The number concentration of EC particles is scaled down to enhance the computational efficiency. As long as the evaporation and condensation effect is considered to be negligible, the reduced total number of particles injected will have no impact on the accuracy of simulation results. A random-parabolic particle distribution was generated at the inlet, by an in-house MATLAB code (Feng et al., 2016).

For EC vapor species, the puffing topography presented by CORESTA (2014) has been used in the experiment by Margham et al. (2016). Data are also provided for the lab environment air known as a blank aerosol. In this study, the composition of the aerosol vapor is determined by the subtraction of the existing chemicals in the air. Moreover, the change in composition caused by different puff volumes (55 and 80 ml) was reported in the same work. The data are not provided for the volatile organics and nicotine. By considering the constant density for unavailable chemicals, the generated vapor composition is calculated. As long as the mass fraction of the formaldehyde and acrolein in the generated aerosol is much lower than other components, the influence of the puff volume on the aerosol composition is negligible. Additional data are provided in Table S.1.

Nonslip boundary conditions are applied for airflow at the airway walls. The deposition of the chemicals is happening in two forms of vapor phase and the particle phase. For discrete particles, 100% trapped wall is implemented due to the presence of mucus layers. Since it is difficult to measure the flow or pressure at each airway outlets the uniform pressure outlet boundary condition with gauge pressure equal to zero is employed.

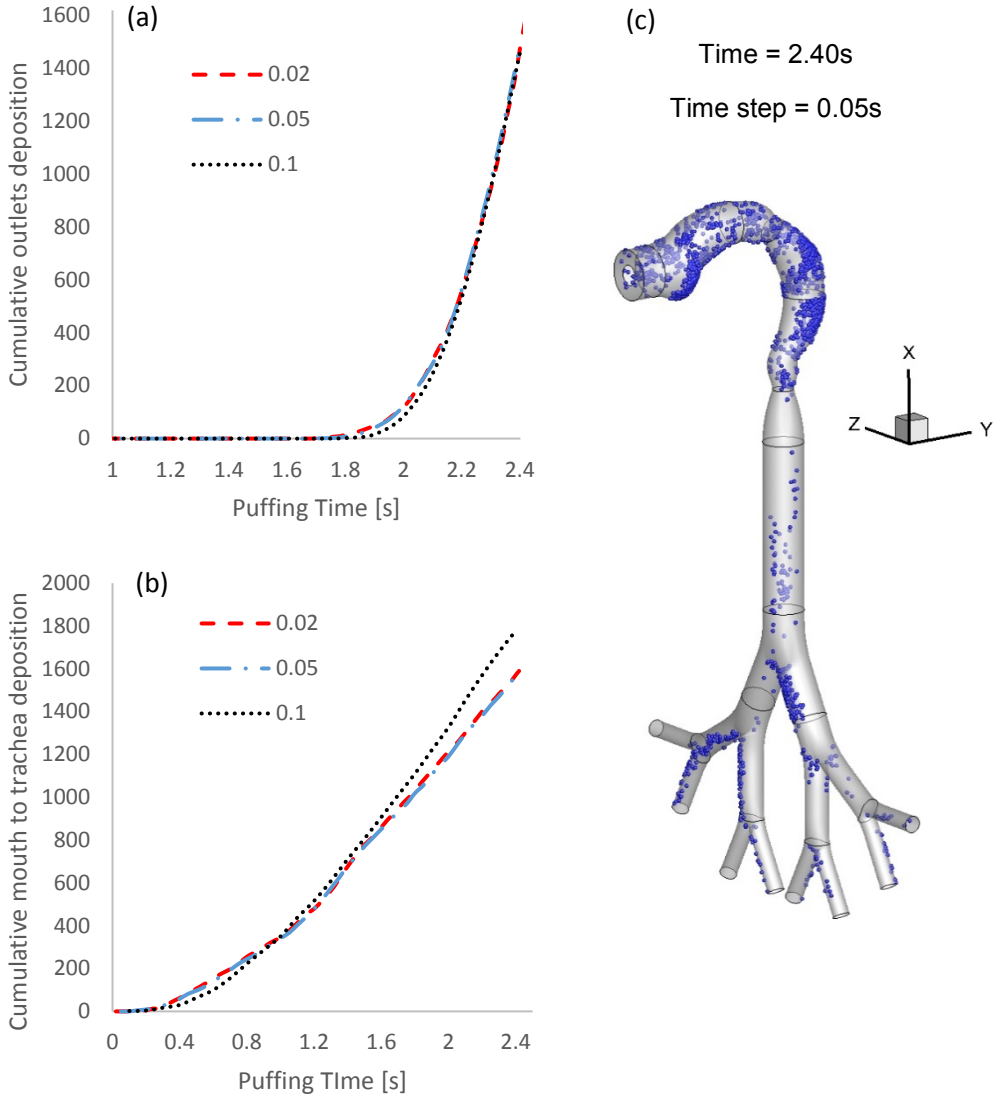

Figure S.1. Cumulative particle deposition and escape numbers in the idealized human upper airway model for particle injection independence test: (a) particle escaping number at outlets (b) particle deposition number from mouth to trachea (c) particle deposition patterns at t=2.4 s

S.1.2 Physiologically Based Toxicokinetic (PBTK) Model

The biological sketch of the compartments being considered in the present PBTK model is shown in Figure 1. There are two major types of PBTK models, i.e., perfusion-limited and diffusion-limited (Rosenbaum, 2016). Based on the lipophilic (hydrophilic) characteristics of nicotine and acrolein, flow-limited diffusions are dominant through all the compartments (Robinson et al., 1992). Furthermore, the division of compartments depends on the focus and goal of different studies. Since the PBTK model is designed to be combined with the CFPD model, the inputs of the nicotine and acrolein uptakes will be obtained from the lung deposition data. In the following equations, subscripts T and M represent "tissue"

and "metabolizing sites of hepatic or renal" respectively. The generalized time-dependent ordinary differential equation (ODE) for the perfusion-limited model can be given as:

$$V_T \frac{d}{dt} C_T = Q_T \cdot \left(C_{T,in} - \frac{C_T}{K_T} \right) - IC_M \frac{C_T}{K_T} \quad \text{(S20)}$$

For eliminations in the systemic region, the intrinsic hepatic clearance (IC_H) and intrinsic renal clearance (IC_R) are considered for liver and kidney, respectively. Apparently, the elimination term is equal to zero for the non-eliminating organs. For tissues other than the venous pool, arterial pool, lung, and liver the input concentrations $C_{T,in}$ are equal to arterial pool concentrations. Moreover, the input concentration for the venous pool is the average amalgamation of interconnected organs, which can be given by:

$$C_{inlet} = \frac{1}{Q_{venous}} \sum_T Q_T \, (C_T / K_T) \quad \text{(S21)}$$

where Q_{venous} is the cardiac output which represents total blood circulation flow rate, which is identical for venous, arterial, and lung. For the liver, the same procedure as venous inlet can be used by combining gastrointestinal tract and arterial pool concentrations.

The accuracy of a PBTK model relies on the determination of parameters of each compartment including tissue volume, flow rate, blood-tissue partition coefficient, and alveolar flow rate at rest. Parameter values used in this study are listed in Table S.2 (Ramsey & Andersen, 1984; Robinson et al., 1992). The optimized values for the renal and hepatic clearances are obtained from the validation that are tabulated in Table S.5. To provide reliable predictions of toxicant translocations, we have optimized and validated the PBTK model by comparing our numerical predictions with the toxicant-plasma concentration data acquired from benchmark open literature (please see model validation).

S.1.3 Interconnection Model between CFPD and PBTK

Mucus, epithelial, and subepithelial layers consist the barrier between lung and blood circulation. The interconnection model between CFPD and PBTK models presented in this study is addressed in the following. One-way exchange from the lung to blood is assumed due to the negligible amount of toxicants reentering the lung from the blood circulation. Bush et al. (1998) and Corley et al. (2012 & 2015) used the physiological configuration concept of the mucosa bed including the mucus, epithelial, and subepithelial layers. Considering no reaction in the layers make it possible to use Henry's law of vapor-liquid equilibria for estimating the uptake magnitude due to vapor phase deposition (Smith, Van Ness, & Abbott, 1996). The air and mucus phase diffusivity and Henry's law constant for the chemicals presented in this study are listed in Table S.3.

To estimate the available vapor species concentration entering the systemic regions based on the absorption rate predicted by the CFPD model and boundary conditions, the regional area weighted average mass fraction $Y_{S,R}$ can be given as:

$$Y_{s,R} = \frac{\sum_{cells} Y_s A_c}{\sum_{cells} A_c} \quad \text{(S22)}$$

In Eq. (S22), subscript R represents "Region". For calculation of the vapor species uptake concentration ($C_{VU,s}$), the following equation is utilized:

$$C_{VU,s} = \sum_R f_{R,V,s} \frac{0.05\, Y_{s,R}\, \rho\, (puff\ volume)}{3\, A_R\, H_m} \quad \text{(S23)}$$

where 0.05 denotes to the selected CFPD simulation time step, A_R is the region surface area and $f_{R,V,s}$is the regional bioavailability factor provided in Table S.4. The lymph vein compartment connecting with the lung is assumed as a layer with a constant thickness (H_m). The surface area of the regions are provided in Table S.4.

Table S.2 Physiochemical parameters of tissues, renal and hepatic clearances optimized for nicotine translocation.

Compartment Name	Volume [L]	Blood Flow [L/min]	Blood-Tissue Partition Coefficient
Arterial Pool	1.4	6.1	1
Venous Pool	4	6.1	1
Muscle Group	34.4	1.65	2.5
Fat Group	10	0.3	1
Vessel-rich Group	1.55	1.35	3
Gastrointestinal tract	2.4	1.25	2
Liver	1.5	0.3	9
Kidney	0.3	1.25	15
Lung	0.6	6.1	2

Table S.3. Properties of nicotine and acrolein in vapor forms.

Species (s)	$D_{a,s}$ [cm^2 /s]	$D_{w,s}$ [cm^2 /s]	$H_{c,s}$	Ψ_s [cm^{-1}]
Acrolein	0.105	1.1200E-05	4.9866E-03	2.1391E+03
Formaldehyde	0.18	2.0000E-05	1.3775E-05	8.0664E+05
Nicotine	0.065	8.6000E-06	5.5997E-08	2.3627E+08
VG	0.0877	9.3000E-06	7.0712E-07	1.4996E+07
PG	0.106	1.2300E-05	5.3136E-07	2.1838E+07

For the diffusion of the chemical compounds due to particle depositions, the transient regional number of deposited particles are recorded by considering the wall boundaries as 100% trapped wall. The species uptake concentration $C_{pU,S}$ due to particle deposition is calculated by:

$$C_{pU,s} = \sum_R f_{R,p,s}\, SC\, \frac{nD_R\, \rho_{p,s}\, \pi d_p^3}{6\, A_R\, H_m} \quad \text{(S24)}$$

where SC= 1.0e+7 is the scaling factor selected to enhance the computational efficiency without losing

precision. Specifically, particle numbers injected per time step are multiplied by SC, so that the regional particle number deposition (nD_R) reflects the actual number of particles carried by the generated aerosol. The bioavailability factors for the particle phase is provided in Table S.4. It should be noted that these fractions will justify the influence of the lymph vein distribution concentration; diffusion, and reaction of the species.

Table S.4. The surface area of the regional sections and bioavailability factors of the idealized human upper airway.

Region Number	Name	Area [cm^2]	Bioavailability Factors		
			EC Particles	Nicotine in Vapor	Acrolein in Vapor
Region 1	Oral Cavity	0.3545	9	0.39	0.14
	Oropharynx/Larynx	0.4151	9	0.39	0.14
Region 2	Trachea	0.424	12	0.79	0.29
Region 3	G1 (Primary Bronchi)	0.2984	17	1.99	0.49
	G2	0.5209	17	1.99	0.49
	G3	0.4666	17	1.99	0.49

Therefore, adding Eqs. (S23) and (S24) yields the total uptake concentration of the chemical compound. An example of concentration time course is shown in Figures 8 (a) and (b). To quantify the average administration of toxicants, the area under the curve (AUC) and the time step size need to be known. The average uptake concentration can be calculated by:

$$AUC = \frac{\int_{t_1}^{t_2} C_{T,inlet}}{t_2 - t_1} \tag{S25}$$

In this study, the only input source of toxicants is from the EC aerosol inhalation via the pulmonary route. Dermatological absorption can be neglected. Additionally, by assuming that the equilibrium will always hold between inhaled air and the pulmonary blood circulation, the material mass balance equation for toxicants can be given as:

$$C_{arterial} = \frac{\dot{Q}_{lung} C_{uptake} + \dot{Q}_{venous} C_{venous}}{\dot{Q}_{venous} + \dot{Q}_{lung}} \tag{S26}$$

where C_{uptake} is the deposition concentration predicted by the CFPD model.

S.2. Geometry and Mesh Independence Test

S.2.1 Idealized Human Upper Airway Model

In this study, an idealized upper human respiratory airway from the oral cavity to G3 with eight outlets is selected. The structure dimensions are based on the sizes presented by Cheng, Zhou, and Chen (1999) with a revised 8-mm mouth opening (see Figure 1). Despite the simplification of the geometry, it contains most important anatomical features of the human upper airway that is essential in the study of the EC aerosol deposition and mass exchange at airway walls. Based on

the physiological characteristics of the respiratory system, the current geometry has been divided into three sections based on the thickness of the mucus layer in different regions and also the existence of the lymph veins after the sub-epithelium layer. Region 1 includes the oral cavity and the pharynx with the thickest mucus layer and lowest lymph vein concentration. Region 2 is the trachea with lower thickness and the higher existence of the lymph vein connected to the tissue. Region 3 consists of the tracheobronchial tree from G1 to G3 with the lowest mucus layer thickness and the highest lymph vein concentration (see Table S.4).

S.1.2. Hexahedral Mesh Generation and Mesh Independence Test

Computational meshes were generated, using the commercial software ICEM CFD v. 18.0 (ANSYS Inc., Canonsburg, PA). The structured, multi-block mesh developed with the feature of hexahedral elements and refinement at the wall boundaries. The final mesh has the total elements number of 2,374,679, with 2,319,768 nodes. The mesh independence test has been performed by Feng et al. (2016) with the inlet volumetric flow rate of 27.5 ml/s. The mesh topology was determined by refining the mesh until grid independence of the flow field solution was achieved.

S.2.2 Numerical Setup

The numerical solution of the governing equations with appropriate boundary conditions was achieved by using a user-enhanced, commercial finite-volume based program, i.e., ANSYS Fluent and CFX 18.0 (ANSYS Inc., Canonsburg, PA). All variables, including velocity components, pressure, turbulence variables and particle trajectories and deposition data are calculated and located at the centroids of the discretized mesh cells. Numerical simulations were performed on a local 64-bit Dell Precision T7910 workstation with 256 GB RAM and sixteen 3.1GHZ CPUs and the supercomputers in High Performance Computing Center at Oklahoma State University (e.g., Cowboy cluster machine with 252 standards compute nodes with dual Intel Xeon E5-2620 “Sandy Bridge” hex core 2.0 GHz CPUs, with 32 GB of 1333 MHz RAM). A second-order upwind scheme was used for the momentum equation calculation. For the calculation of the species transport, the first order upwind was employed, and for the pressure and velocity coupling in the finite volume solver, the semi-implicit method for pressure-linked equations (SIMPLE algorithm) has been selected. The system of ODEs of the PBTK model was solved using the 4^{th} order Runge–Kutta method. The PBTK model has been written in C language in the form of user-defined functions (UDFs) and was attached to the CFPD model in ANSYS Fluent 18.0. As a result

at each puff, the translocation of the current toxicants has been tracked in the systemic region. The time delay of the translocation was neglected.

S.3. Model Validations

S.3.1 CFPD Model Validations

For particle dynamics model validations, regional deposition efficiencies (RDEs) were compared with benchmark experimental data in the idealized upper airway geometry (see Figure 1) with 1-cm mouth inlet (Cheng et al., 1999). The inlet conditions with uniform velocity condition and the volumetric flow rates of 15, 30, and 60 L/min are applied for the polystyrene latex fluorescent particles. As shown in Figure S.2 (a), the extrathoracic RDE is a function of impaction parameter d_p^2Q [μm^2 L min^{-1}]. The empirical curve and the numerical results show good agreement in mouth-to-throat RDE. The total DE of the present model sufficiently reaches an agreement with the published literature. Additionally, comparisons with experimental deposition data at various flow rates are plotted in Figure S.2 (b). The numerical data also show the same trend for the particles in the same range. For the micro-particles, DF increases with the increased particle diameter due to the enhanced inertial impaction. In contrast, higher RDEs are observed for nanoparticles compared to submicron particles due to the enhanced Brownian motion. Furthermore, Figure S.2 (c) shows additional deposition data comparisons with good agreements. In summary, the CFPD model is well validated.

S.3.2 PBTK Model Optimizations and Validations

S.3.2.1 Nicotine

For nicotine PBTK model validation, plasma concentration vs. total volume is compared and presented in Figure S.3. The details of this experiment are provided in Table S.5. Benchmark experimental data of nicotine plasma concentrations due to CC smoking scenarios (Benowitz, Jacob, Jones, & Rosenberg, 1982; Kyerematen, Morgan, Chattopadhyay, Bethizy, & Vesell, 1990) were employed first and used for two independent model validations for nicotine PBTK. Two different mass flow rates of nicotine infusion were employed, i.e., 40 μg/min for 30 minutes and 95 μg/min for 2 minutes. The PBTK model was also compared with nicotine plasma concentration data of an EC study by Dawkins et al. (2016). Specifically, E-liquid with 6-24 ng/ml nicotine has been used on 11 volunteers for 60 minutes, who was abstained from smoking for 6 hours before the clinical test. Additionally, numerical results generated by another PBTK model (Robinson et

al., 1992) is also included in Figure S.3. Employing the parameters provided by Dawkins et al. (2016), our nicotine PBTK predictions show good matches with experiments.

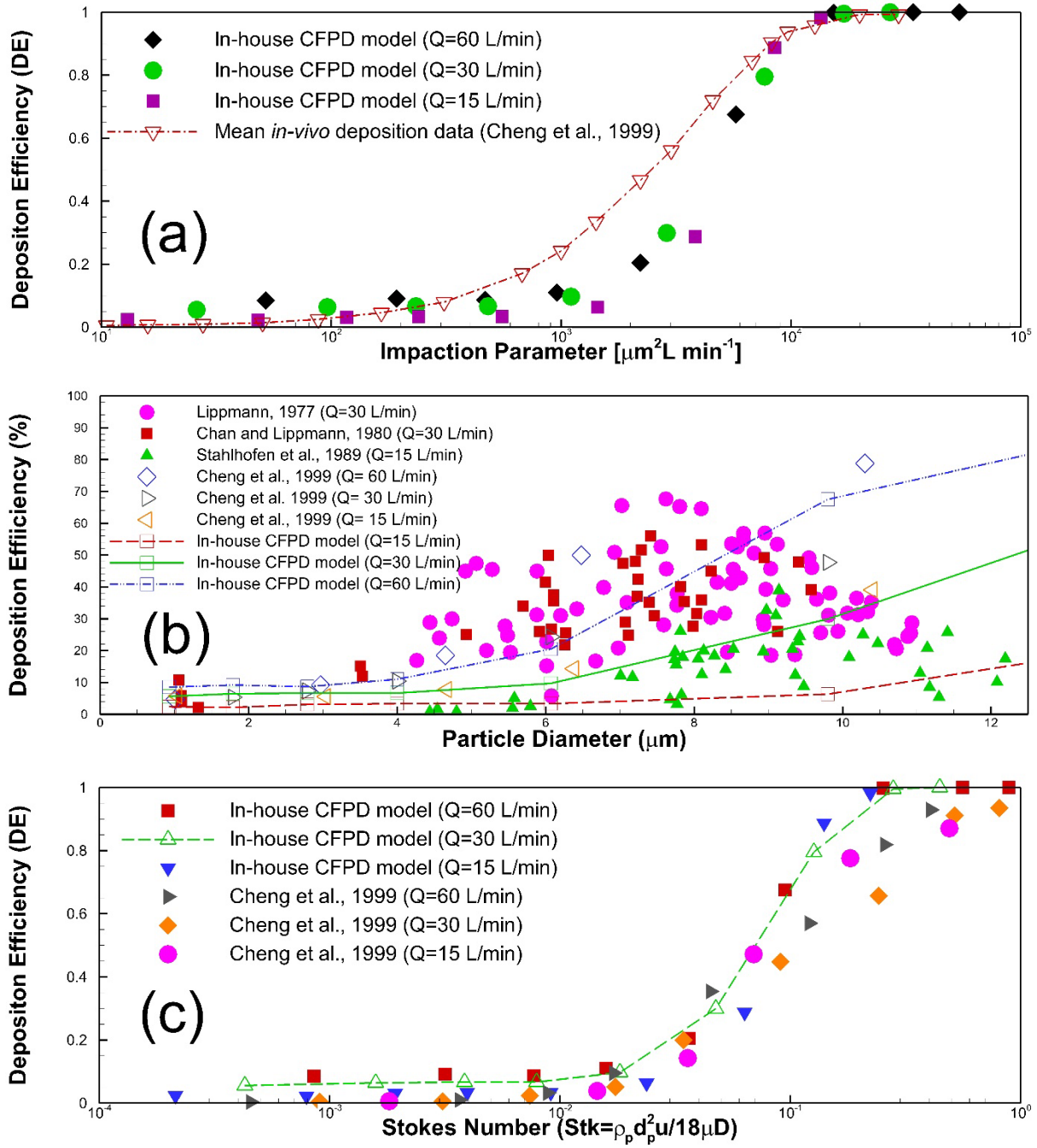

Figure S.2. CFPD model validations: (a) deposition efficiency comparisons in the oral cavity with different mean impaction parameters (b) deposition efficiency comparisons in the oral cavity for different particle sizes (c) deposition efficiency comparisons in the oral cavity with different Stokes numbers.

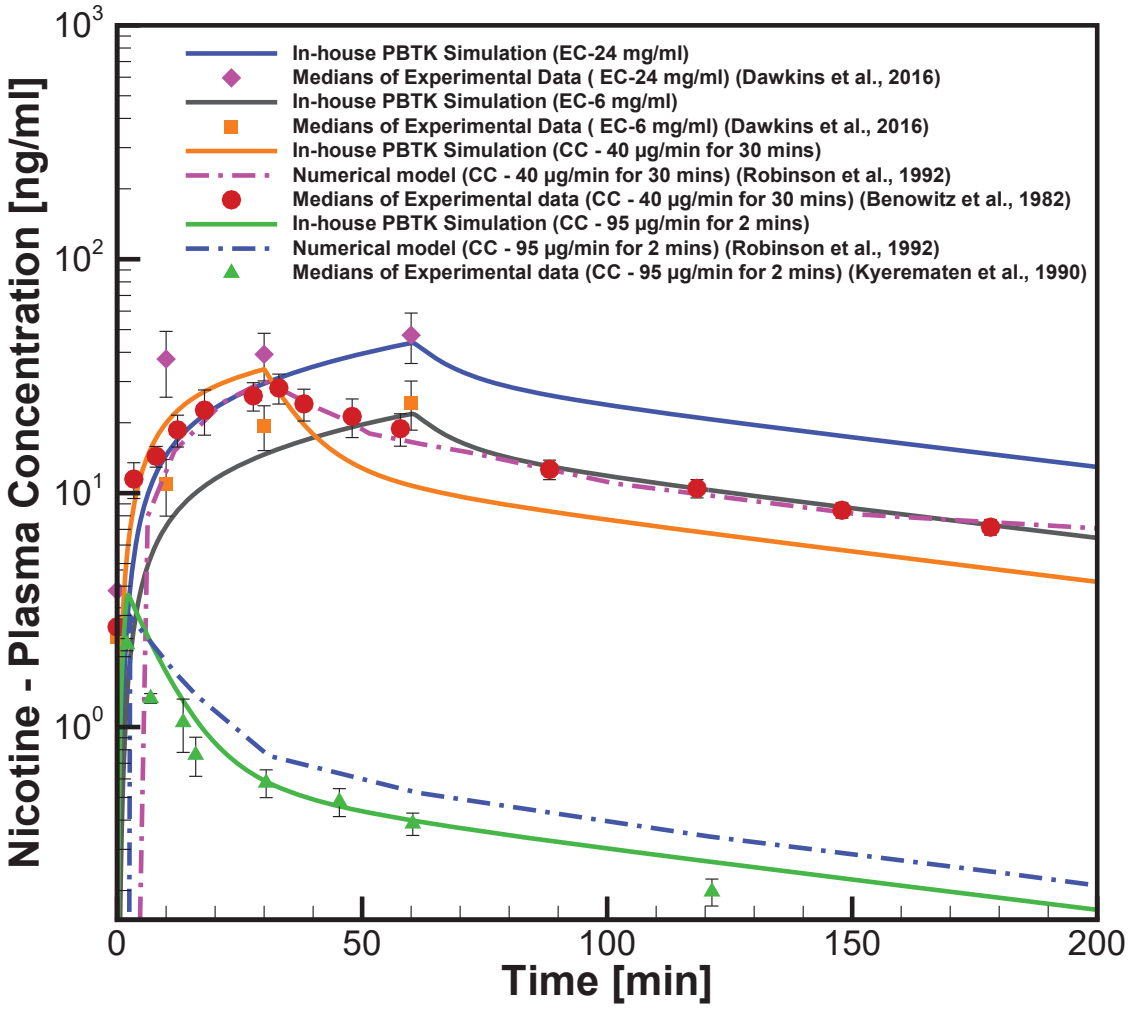

Figure S.3. Nicotine PBTK model optimization and validations.

S.3.2.2 Acrolein

Exposure to acrolein in human body has not been investigated due to the invasive nature of the test methodology (Agency for Toxic Substances and Disease Registry, 2007). Animal studies (F-344 rat, mice) are employed in this study. There is a need to employ a scale-up factor from animal to human body based on the weight differences. The time scaling-up equation proposed and validated by Bailey et al. (1989) and Kreyling et al. (1998) are used to convert the animal data to human organ volume size.

$$Time_{human}/Time_{animal} = \left(Body\ Weight_{human}/Body\ Weight_{animal}\right)^{0.275} \quad \text{(S27)}$$

For the comparison, data of creatinine with a density of 0.0024 mg/ml and 3-HPMA for 1 and 0.5 ppm inhalation of the pure acrolein by Conklin et al. (2017) in mice is introduced. To scale

up between species, the weight comparison of 73 kg (human)/0.23 kg (mice) are quoted in the clearance phase. The optimized values of the hepatic and renal clearances are investigated for the case of the 1.0-ppm exposure, and the same values are employed for the comparison of the case with the 0.5-ppm exposure. As it is shown in Figure S.4, the increase in intake amount shift the concentration profile to higher maximum uptake, and the clearance process of the higher concentration of the intake concentration is higher than the lower intake exposure.

Table S.5. Benchmark experimental data on nicotine translocations for the nicotine PBTK model optimization and validation.

Volunteers	EC Products	Nicotine Solution	Exposure	Uptakes	Puffing topography	Reference
11 (11 male)	eVic™ supreme, with Nautilus Aspire tank, 3.9 V (8.5 W)	6-24 mg/mL	60 min ad libitum	nicotine concentrations of 8.59, 16.99, and 22.03 ng/mL at 10, 30 and 60 min	Mean number of puff: 70.73; Puff duration: 5.20 s	Dawkins et al. (2016)
				nicotine concentrations of 33.77, 35.48, and 43.57 ng/mL at 10, 30 and 60 min	Mean number of puff: 48.26; Puff duration: 3.84 s	
16 (15 male)	cartomizer, 3.3 V; 1.5 Ω (7.26 W)	8 mg/ml	2 bouts with duration of 10min; 10 puff; puff restriction on users	Bout 1: peak nicotine concentration 17.8 ng/ml	Bout 1: Mean puff volume: 208.4 ml; Puff duration: 6.1 s; Bout 2: Mean puff volume: 176 ml; Puff duration: 5.5 s	Ramôa et al. (2015)
				Bout2: peak nicotine concentration 16.9 ng/ml		
		18 mg/ml		Bout 1: peak nicotine concentration 25.9 ng/ml	Bout 1: Mean puff volume: 124.2 ml; Puff duration: 5.35 s; Bout 2: Mean puff volume: 114.7 ml; Puff duration: 4.97 s	
				Bout2: peak nicotine concentration 23.6 ng/ml		
		36 mg/ml		Bout 1: peak nicotine concentration 36 ng/ml	Bout 1: Mean puff volume: 84.3 ml; Puff duration: 4.17 s	
				Bout2: peak nicotine concentration 24.7 ng/ml	Bout 2: Mean puff volume: 78.5 ml; Puff duration: 3.98 s	

The experience as the relative definition and influencing factor of acrolein uptake have been investigating in the study by Struve et al. (2008). Two groups of pre-exposed and naïve F344 rats are exposed to acrolein through inhalation and the influence of the parameters of acrolein concentration (0.6, 1.8 and 3.6 ppm) and constant velocity unidirectional inspiratory flow rate (100 and 300 ml/min) for 80 min exposure on the acrolein and glutathione uptake efficiency on upper respiratory are investigated. The experienced rats were previously exposed to acrolein for 6 hrs/day, 5 days/week in 14 days duration.

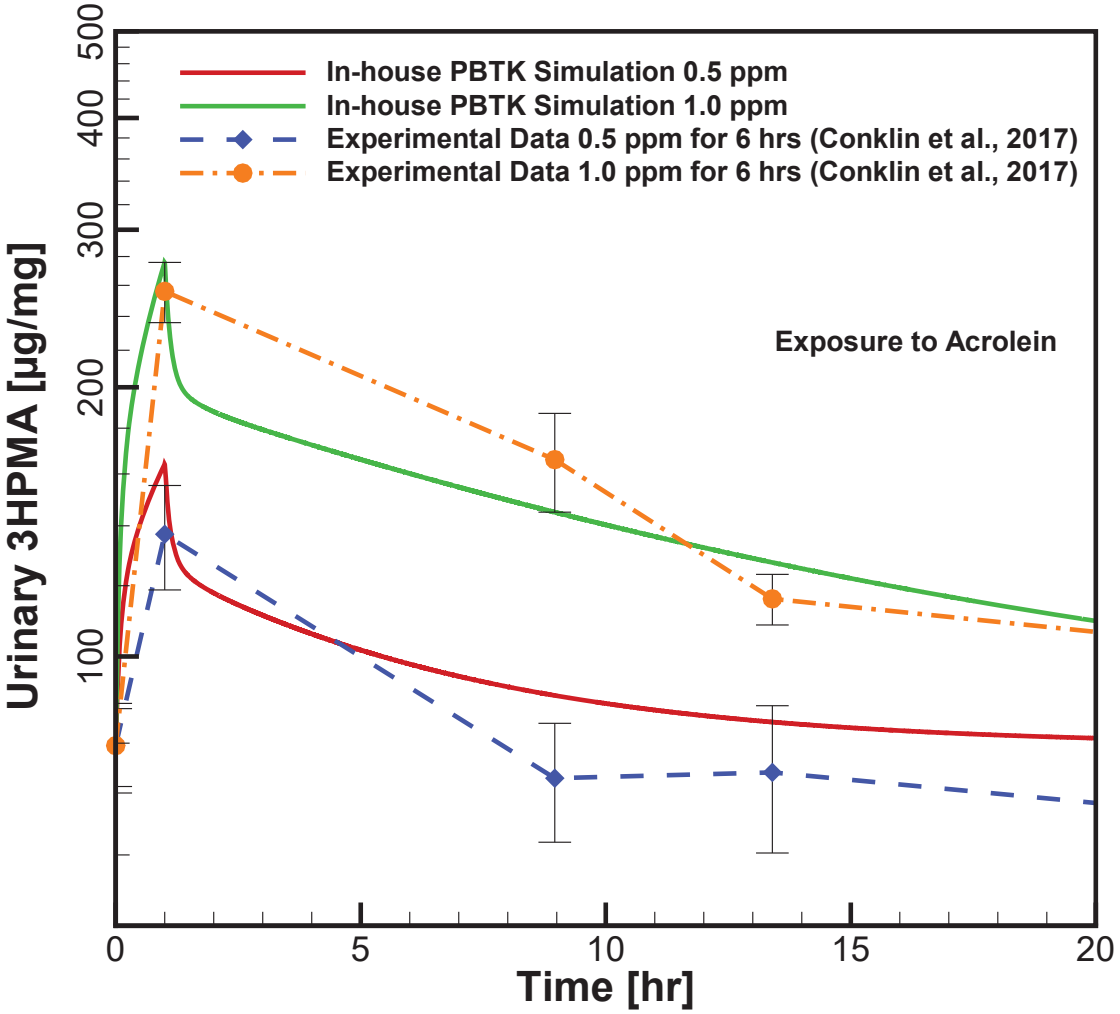

Figure S.4. Acrolein PBTK model optimization and validations by the comparisons of 3-HPMA concentration in rats.

Studies on acrolein inhalation exposure on an animal show no significant change on the hepatic and renal processes. It was proposed that liver weight will relatively increase in rats in the long-term exposure of 60–180 days (Kutzman, Wehner, & Haber, 1984). A similar pattern was investigated for an increase in kidney size in rats and hamsters exposed to 4–5 ppm for 60-

90 days (Kutzman, Popenoe, Schmaeler, & Drew, 1985). All in all the assumption for constant renal and hepatic clearance function seems reasonable. The optimized values of the renal and hepatic clearances of acrolein and nicotine are provided in Table S.6.

Table S.6. Optimized parameter values of hepatic and renal clearances.

Chemical – Case of Optimization	Renal intrinsic clearance (IC_R) [L/min]	Hepatic intrinsic clearance (IC_H) [L/min]
Nicotine (Robinson et al., 1992)	0.1700	1.0900
Acrolein (Conklin et al., 2017)	0.2260	0.9460

S.4. Limitations of the Study

Due to the complexity of the realistic EC aerosol dynamics in the human body, limitations exist for the current CFPD-PBTK simulations. The assumptions employed are:

(1) Spherical particle with constant diameter is assumed

(2) The effect of evaporation/ condensation is neglected.

(3) The deposition and uptake due to exhalation cycle are not simulated.

(4) The complete conversion of the acrolein to 3-HPMA is not modeled.

(5) The cotinine as the main metabolite of the nicotine is not modeled in PBTK simulation.

(6) The bioavailability factors have been used to connect the CFPD to PBTK models. This fraction was hypothesized to combine the influence of the reaction, diffusion and the lymph vein concentration at regional contact with the lung tissue.

(7) Square waveforms are selected as puffing inlet conditions.

(8) The time delay effect of the closed loop system of the human body organs configuration is not considered.

References

Allen, M. D., & Raabe, O. G. (1985). Slip correction measurements of spherical solid aerosol particles in an improved Millikan apparatus. *Aerosol Science and Technology, 4*(3), 269-286.

ATSDR. (2007). Toxicological Profile for Acrolein. In A. f. T. S. D. Registry (Ed.): US Department of Health and Human Services, Public Health Service Atlanta, GA.

Bailey, M., Kreyling, W., Andre, S., Batchelor, A., Collier, C., Drosselmeyer, E., . . . Hodgson, A. (1989). An interspecies comparison of the lung clearance of inhaled monodisperse cobalt oxide particles—Part I: Objectives and summary of results. *Journal of aerosol science, 20*(2), 169-188.

Behar, R. Z., & Talbot, P. (2015). Puffing topography and nicotine intake of electronic cigarette users. *PLoS One, 10*(2), e0117222.

Benowitz, N. L., Jacob, P., Jones, R. T., & Rosenberg, J. (1982). Interindividual variability in the metabolism and cardiovascular effects of nicotine in man. *Journal of Pharmacology and Experimental Therapeutics, 221*(2), 368-372.

Bush, M. L., Frederick, C. B., Kimbell, J. S., & Ultman, J. S. (1998). A CFD–PBPK hybrid model for simulating gas and vapor uptake in the rat nose. *Toxicology and applied pharmacology, 150*(1), 133-145.

Cheng, Y.-S., Zhou, Y., & Chen, B. T. (1999). Particle deposition in a cast of human oral airways. *Aerosol Science & Technology, 31*(4), 286-300.

Conklin, D. J., Malovichko, M. V., Zeller, I., Das, T. P., Krivokhizhina, T. V., Lynch, B. H., . . . Haberzettl, P. (2017). Biomarkers of Chronic Acrolein Inhalation Exposure in Mice: Implications for Tobacco Product-Induced Toxicity. *Toxicological Sciences*.

CORESTA. (2014). Routine analytical machine for e-cigarette aerosol generation and collection - definitions and standard conditions. *CORESTA recommended method No. 81*.

Corley, R. A., Kabilan, S., Kuprat, A. P., Carson, J. P., Jacob, R. E., Minard, K. R., . . . Glenny, R. (2015). Comparative risks of aldehyde constituents in cigarette smoke using transient computational fluid dynamics/physiologically based pharmacokinetic models of the rat and human respiratory tracts. *Toxicological Sciences, 146*(1), 65-88.

Corley, R. A., Kabilan, S., Kuprat, A. P., Carson, J. P., Minard, K. R., Jacob, R. E., . . . Cox, T. (2012). Comparative computational modeling of airflows and vapor dosimetry in the respiratory tracts of rat, monkey, and human. *Toxicological Sciences, 128*(2), 500-516.

Dautzenberg, B., & Bricard, D. (2015). Real-time characterization of e-cigarettes use: the 1 million puffs study. *J Addict Res Ther, 6*(2).

Dawkins, L. E., Kimber, C. F., Doig, M., Feyerabend, C., & Corcoran, O. (2016). Self-titration by experienced e-cigarette users: blood nicotine delivery and subjective effects. *Psychopharmacology, 233*(15-16), 2933-2941.

Drew, D. A. (1976). Two-phase flows: constitutive equations for lift and Brownian motion and some basic flows. *Archive for Rational Mechanics and Analysis, 62*(2), 149-163.

Feng, Y., Kleinstreuer, C., Castro, N., & Rostami, A. (2016). Computational transport, phase change and deposition analysis of inhaled multicomponent droplet–vapor mixtures in an idealized human upper lung model. *Journal of aerosol science, 96*, 96-123.

Farsalinos, K. E., Voudris, V., & Poulas, K. (2015). E-cigarettes generate high levels of aldehydes only in 'dry puff'conditions. Addiction, 110(8), 1352-1356.

Goniewicz, M. L., Knysak, J., Gawron, M., Kosmider, L., Sobczak, A., Kurek, J., . . . Havel, C. (2013). Levels of selected carcinogens and toxicants in vapour from electronic cigarettes. *Tobacco control*, tobaccocontrol-2012-050859.

Gupta, D., & Peters, M. H. (1985). A Brownian dynamics simulation of aerosol deposition onto spherical collectors. *Journal of Colloid and Interface Science, 104*(2), 375-389.

ICRP. (1994). Human respiratory tract model for radiological protection. *ICRP publication 66. Annals of the ICRP, 24*, 1-3.

ISO. (2015). ISO/TR 19478-2. ISO and Health Canada intense smoking parameters - Part 2: Examination of factors contributing to variability in the routine measurement of TPM, water and NFDPM smoke yields of cigarettes.

Kyerematen, G. A., Morgan, M. L., Chattopadhyay, B., Bethizy, J. D., & Vesell, E. S. (1990). Disposition of nicotine and eight metabolites in smokers and nonsmokers: identification in smokers of two metabolites that are longer lived than cotinine. *Clinical Pharmacology & Therapeutics, 48*(6), 641-651.

Kreyling, W., Hodgson, A., Guilmette, R., Scarlett, C., Badmin, A., & Stradling, G. (1998). Interspecies comparison of lung clearance using monodisperse terbium oxide particles. *Radiation protection dosimetry, 79*(1-4), 241-243.

Kutzman, R. S., Popenoe, E. A., Schmaeler, M., & Drew, R. T. (1985). Changes in rat lung structure and composition as a result of subchronic exposure to acrolein. *Toxicology, 34*(2), 139-151.

Kutzman, R. S., Wehner, R. W., & Haber, S. B. (1984). Selected responses of hypertension-sensitive and resistant rats to inhaled acrolein. *Toxicology, 31*(1), 53-65.

Li, A., & Ahmadi, G. (1992). Dispersion and deposition of spherical particles from point sources in a turbulent channel flow. *Aerosol Science and Technology, 16*(4), 209-226.

McAuley, T. R., Hopke, P. K., Zhao, J., & Babaian, S. (2012). Comparison of the effects of e-cigarette vapor and cigarette smoke on indoor air quality. *Inhalation toxicology, 24*(12), 850-857

Margham, J., McAdam, K., Forster, M., Liu, C., Wright, C., Mariner, D., & Proctor, C. (2016). Chemical composition of aerosol from an E-cigarette: A quantitative comparison with cigarette smoke. *Chemical research in toxicology, 29*(10), 1662-1678.

Menter, F., Langtry, R., & Völker, S. (2006). Transition modelling for general purpose CFD codes. *Flow, turbulence and combustion, 77*(1), 277-303.

Menter, F. R., Langtry, R. B., Likki, S., Suzen, Y., Huang, P., & Völker, S. (2006). A correlation-based transition model using local variables—Part I: model formulation. *Journal of turbomachinery, 128*(3), 413-422.

Ramsey, J. C., & Andersen, M. E. (1984). A physiologically based description of the inhalation pharmacokinetics of styrene in rats and humans. *Toxicology and applied pharmacology, 73*(1), 159-175.

Robinson, D. E., Balter, N. J., & Schwartz, S. L. (1992). A physiologically based pharmacokinetic model for nicotine and cotinine in man. *Journal of pharmacokinetics and biopharmaceutics, 20*(6), 591-609.

Robinson, R., Hensel, E., Morabito, P., & Roundtree, K. (2015). Electronic Cigarette Topography in the Natural Environment. *PLoS One, 10*(6), e0129296. doi:10.1371/journal.pone.0129296

Rosenbaum, S. E. (2016). *Basic pharmacokinetics and pharmacodynamics: An integrated textbook and computer simulations*: John Wiley & Sons.

Struve, M. F., Wong, V. A., Marshall, M. W., Kimbell, J. S., Schroeter, J. D., & Dorman, D. C. (2008). Nasal uptake of inhaled acrolein in rats. *Inhalation toxicology, 20*(3), 217-225.

WHO. (2012). Standard operating procedure for intense smoking of cigarettes.